Ternary magnetic semiconductors: recent developments in physics and technology

Vladimir Tsurkan, Hans-Albrecht Krug von Nidda, Alexander Krimmel, Peter Lunkenheimer, Joachim Hemberger, T. Rudolf, Alois Loidl

Angaben zur Veröffentlichung / Publication details:

Tsurkan, Vladimir, Hans-Albrecht Krug von Nidda, Alexander Krimmel, Peter Lunkenheimer, Joachim Hemberger, T. Rudolf, and Alois Loidl. 2009. "Ternary magnetic semiconductors: recent developments in physics and technology." *physica status solidi (a)* 206 (5): 1082–89. https://doi.org/10.1002/pssa.200881137.

Ternary magnetic semiconductors: recent developments in physics and technology

V. Tsurkan[*, 1, 2], H.-A. Krug von Nidda[, 1], A. Krimmel[1], P. Lunkenheimer[1], J. Hemberger[1], T. Rudolf[1], and A. Loidl[1]**

[1] Experimental Physics V, Center for Electronic Correlations and Magnetism, University of Augsburg, Universitätsstraße 1, 86159 Augsburg, Germany
[2] Institute of Applied Physics, Academy of Sciences, str. Academiei 5, 2028 Chişinău, Republic of Moldova

[*] Corresponding author: e-mail vtsurkan@yahoo.co.uk, Phone: +37 322 738171, Fax: +37 322 738149
[**] e-mail hans-albrecht.krug@physik.uni-augsburg.de, Phone: +49 821 598 3114, Fax: +49 821 598 3649

1 Introduction The physics of spinel compounds has experienced a considerable revival of interest during the last decade. The novel phenomena and ground states identified recently in magnetic spinels concern, e.g., the heavy-fermion behaviour in LiV_2O_4 [1, 2], the colossal magnetoresistance at room temperature in $Fe_{0.5}Cu_{0.5}Cr_2S_4$ [3, 4], the composite spin degree of freedom in $ZnCr_2O_4$ [5], the spin dimerization in $CuIr_2S_4$ and $MgTi_2O_4$ [6, 7], the gigantic Kerr rotation [8] and the orbital-glass state in $FeCr_2S_4$ [9, 10], the spin–orbital liquid in $FeSc_2S_4$ [11], the colossal magnetocapacitive effect in $Cd(Hg)Cr_2S_4$ [12, 13], the negative thermal expansion and strong spin-phonon coupling in $ZnCr_2Se(S)_4$ [14–16], and the spin-Peierls-like transitions in $Zn(Cd)Cr_2O_4$ [17–19]. The correlations of charge, spin, and orbital degrees of freedom, which are strongly coupled to the lattice, are thought to be the driving force of this intricate behaviour. Additional complexity arises from the frustration effects related to the topology of the lattice sites occupied by magnetic ions and the competing nearest-neighbour and further-neighbour exchange interactions as well. Magnetic ions residing on the octahedral B-sites form a pyrochlore lattice of corner-sharing tetrahedra, which is known as the most frustrated magnetic lattice [20]. In case of dominating nearest-neighbour antiferromagnetic (AFM) exchange the system alone cannot select a unique ground state and remains in a spin-liquid state down to temperatures much lower than the energy scale provided by the exchange interaction. In these so-called geometrically frustrated antiferromagnets the appearance of magnetic order can result from additional dipole and anisotropic interactions or strong spin–lattice coupling, which lift the spin degeneracy. Large frustration effects were recently also found in a number of sulfide and oxide spinels containing magnetic ions solely on the A-sites [11, 21]. The *A*-site ions form a diamond lattice that can be viewed as consisting of two interpenetrating frustrated *fcc* sublattices shifted by 0.25, 0.25, 0.25 along the ⟨111⟩ direction. Considering the second-neighbour exchange interactions that couple spins within each *fcc* sublattice, frustration effects can be anticipated. Recent theoretical investigations of the exchange interactions in A-site antiferromagnetic spinels demonstrated the decisive role of the second-neighbour

AFM exchange for generating strong frustration effects and predicted a spiral spin-liquid ground state [22].

Here we present a review of results of our recent experimental studies of ternary magnetic oxide and chalcogenide spinels AB_2X_4 (A = Fe, Mn, Co, Cd, Zn, Hg; B = Cr, Co, Sc, Al; X = O, S, Se). Using magnetic susceptibility, specific heat, thermal expansion, electron–spin resonance, neutron diffraction, broad-band dielectric spectroscopy, and infrared (IR) optical spectroscopy, we investigated spin, charge, orbital, and lattice correlations in these compounds. Single crystalline samples grown by different methods and polycrystalline samples prepared with varying stoichiometry were studied. The obtained results provide compelling evidence for the spin liquid, spin–orbital liquid and orbital glass states. The origin of intriguing effects, like colossal magnetocapacitive coupling, negative thermal expansion, and spin-driven Jahn–Teller structural transformations found in these compounds is also discussed.

2 Synthesis, single crystal growth, structural and compositional characterization Developments in the preparative work on ternary sulfides and selenides were aimed on the improvement of their purity and structural quality. Substantial advance was reached by utilization of high-purity starting elements and transport agents. The use of the novel technique of field-activated sintering allows to dramatically accelerate the synthesis procedure, which is the most time consuming step of the crystal preparation [23]. The chemical transport reaction (CTR) is the best technique for the growth of structurally perfect crystals, although the problems of contamination and respective doping by the transport agent have to be taken into consideration. A larger sample dimension can be obtained by flux or liquid transport methods; however the achieved structural quality is lower compared to that grown by CTR. For congruently melting ternary oxides, the travelling heater technique using an image furnace is also giving positive results. Special attention must be paid to compositional and structural characterization. Electron-probe microanalysis was used to check the stoichiometry of each studied sample. High-resolution X-ray synchrotron powder diffraction and high-resolution electron microscopy were used to detect fine structural distortions and symmetry changes.

3 Magnetic, thermal, and IR optical properties

3.1 Spin liquid, spin–orbital liquid and orbital glass Magnetic susceptibility and heat-capacity studies of $MnSc_2S_4$ and $FeSc_2S_4$ reveal strong frustration effects [11]. The $MnSc_2S_4$ compound is a spin-only system with $S = 5/2$, characterized by a spin-frustration parameter $f = |\Theta_{CW}|/T_N \approx 10$. It shows antiferromagnetic order at low temperatures and bears the characteristics of a spin liquid between $T_N = 2.3$ K and 23 K, the latter being the absolute value of the Curie–Weiss temperature $\Theta_{CW} = -23$ K.

The $FeSc_2S_4$ spinel with $S = 2$, $\Theta_{CW} = -45$ K, and Jahn–Teller active Fe^{2+} cations reveals frustration both in the spin and orbital sector. The spin-frustration parameter $f > 900$ is one of the largest ever observed in frustrated magnets. The orbital frustration is evidenced by the magnetic entropy, which significantly exceeds the spin-only value of $R \ln (2S + 1)$ reaching $R \ln 5 + R \ln 2$, with $R \ln 2$ corresponding to the twofold degenerate orbital contribution. Accordingly, $FeSc_2S_4$ was characterized as a spin–orbital liquid below 45 K [11].

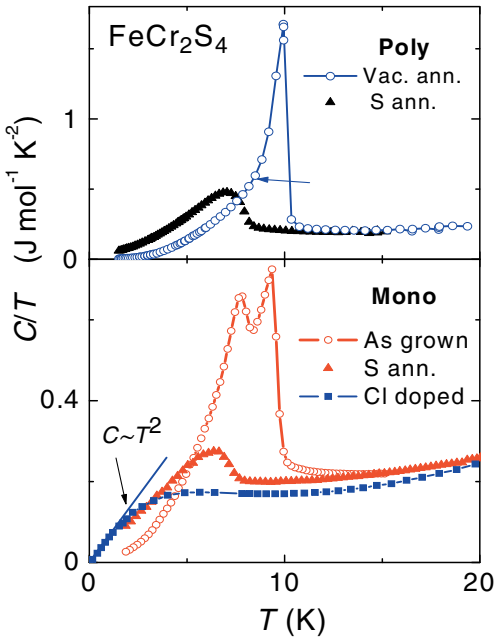

Figure 1 (online colour at: www.pss-a.com) Specific heat in C/T vs. T representation for polycrystalline and single crystalline $FeCr_2S_4$ samples subjected to different annealing and doping. In the as-grown single crystal (prepared by I_2 transport) the orbital-order transition is broadened and split as compared to the vacuum annealed polycrystal.

Insulating $FeCr_2S_4$ with Jahn–Teller active Fe^{2+} cations on the A-site manifests a large linear contribution to the specific heat (~100 mJ/mol K) above the orbital ordering temperature of 10 K (indicated by a λ anomaly) suggesting an orbital liquid state (Fig. 1). In the electronically doped single crystals (prepared by Cl transport) a quadratic term in the specific heat is observed below 3 K down to 50 mK revealing a ground state of an orbital glass [9, 10]. Freezing of the orbital moments in $FeCr_2S_4$ is evidenced also by dielectric spectroscopy which revealed clear relaxational behaviour of the dielectric permittivity exhibiting several features of glassy dynamics [9]. The suppression of the λ anomaly in the specific heat at 10 K in sulphur annealed or electronically doped samples precludes structural disorder as the mechanism of the orbital ordering.

Magnetic susceptibility, electron-spin resonance, and heat-capacity investigations of MAl_2O_4 spinels with M = Co, Fe, and Mn with minor inversion between A- and B-sites reveal spin-glass like ground states for $CoAl_2O_4$ and $FeAl_2O_4$ spinels with freezing temperatures T_f well below the Curie–Weiss temperatures indicating strong frus-

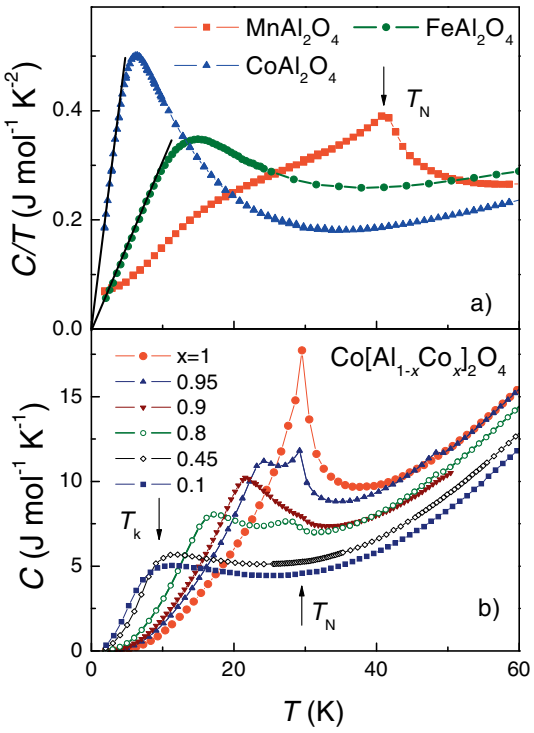

Figure 2 (online colour at: www.pss-a.com) (a) Specific heat in C/T vs. T representation for MAl_2O_4 spinels with M = Co, Fe, and Mn; (b) temperature dependences of C for $Co[Al_{1-x}Co_x]_2O_4$ compositions.

tration [21]. Below T_f, the heat capacities show T^2 temperature dependence for $T \rightarrow 0$ K (Fig. 2a), in contrast to the linear temperature dependence expected for conventional spin glasses. The heat capacity of $FeAl_2O_4$ exhibits an additional orbital contribution. With the absence of a cooperative Jahn–Teller distortion, this points towards a spin–orbital liquid ground state. The specific heat of the $MnAl_2O_4$ compound shows a clear lambda anomaly at 40 K revealing long-range antiferromagnetic order. Magnetic studies and neutron powder diffraction [27] however found a reduced value of the ordered moment and a large paramagnetic component.

The investigation of $Co[Al_{1-x}Co_x]_2O_4$ spinels with only magnetic A-site Co^{2+} ions reveals large negative Curie–Weiss temperatures Θ_{CW} of the order of –110 K independent of substitution, which is attributed to a high multiplicity of the superexchange interactions between the Co cations [24]. A pure antiferromagnetic state is found for $x = 1.0$ with the Néel temperature $T_N = 29.5$ K as evidenced by a lambda-like anomaly in the specific heat (Fig. 2b). With decreasing x a strong reduction of T_N is observed. For $x \leq 0.2$ a T^2 dependence of the specific heat and a spin-glass like behaviour of the susceptibility are detected below $T_f \sim 4.7$ K. The high value of the frustration parameter $f = |\Theta_{CW}|/T_f > 10$ indicates strong spin frustration. The frustration mechanism is attributed to competing nearest-neighbour and second-neighbour superexchange interactions between the A-site Co^{2+} ions. For $0.2 \leq x \leq 0.75$ at low temperatures, a $T^{2.5}$ dependence of the specific heat is indicative of a spin-liquid state [22].

3.2 Neutron-scattering evidence of the spin-liquid and spin–orbital liquid states The electronic part of the specific heat in frustrated $FeSc_2S_4$ is composed of a spin and an additional orbital contribution. Combined with the absence of any phase transition above 50 mK this provides strong evidence for a spin–orbital liquid state [11]. This is confirmed by inelastic neutron scattering. The results demonstrate that the orbital doublet remains degenerate but is strongly coupled to vibronic modes with a vibronic splitting $\Gamma = 2$ meV. This excitation can be explained in terms of a dynamic Jahn–Teller effect including spin–orbit coupling. Spin excitations of the liquid state show a strong dispersion with a spin gap of 0.2 meV [25]. The spin system reveals a crossover from a system with strong AFM spin fluctuations with a purely relaxational excitation spectrum at $T > 2|\Theta_{CW}|$ to a cooperative paramagnet with isotropic magnon-like excitations at low temperatures ($T < |\Theta_{CW}|$). The orbital disorder is suggested to play an essential role in establishing the spin-liquid state.

In spin-frustrated $MnSc_2S_4$ neutron powder diffraction shows a complex spiral arrangement in the a–b plane with a propagation vector (3/4, 3/4, 0). The magnetic structure is achieved via a complex multi-step ordering process characterized by incommensurate modulation at $T_{N1} = 2.3$ K and a locked-in commensurate structure below the second transition at $T_{N2} = 1.9$ K [26]. Despite the presence of strong antiferromagnetic interactions as reflected in a Curie–Weiss temperature of $\Theta_{CW} = -23$ K, the long-range magnetic order is suppressed down to a transition temperature $T_{N1} = 2.3$ K revealing a broad spin-liquid regime for $T_{N1} < T < |\Theta_{CW}|$. The magnetic excitation spectra show a quasielastic response with a width of the order of 1 meV corresponding to the magnetic energy scale. Upon approaching the long-range magnetic order, a change from quasielastic to inelastic magnetic response is observed. The magnetic structure of $MnSc_2S_4$ therefore shows a transition from a high-temperature paramagnet for $T > |\Theta_{CW}|$ via a spiral spin-liquid phase for intermediate temperatures $T_N < T < |\Theta_{CW}|$ to magnetically long-range ordered ground state for low temperatures $T < T_N$.

Neutron diffraction studies were performed on the A-site spinels MAl_2O_4 (M = Co, Fe, Mn). Whereas the Mn-based compound representing a spin-only system shows long-range antiferromagnetic order below $T_N = 40$ K with a simple collinear magnetic structure, the diffraction patterns of the Fe and Co spinels reveal a characteristic liquid-like structure factor of the magnetic scattering [27]. Inelastic neutron scattering experiments on these compounds elucidated the corresponding magnetic excitations. $MnAl_2O_4$ was found to exhibit the strongest magnetic exchange. Its long-range magnetic order is reflected by well defined spin-wave dispersion (uppermost frame of Fig. 3). For $CoAl_2O_4$, inelastic neutron scattering shows a dispersion-like structure indicating collective magnetic excitations de-

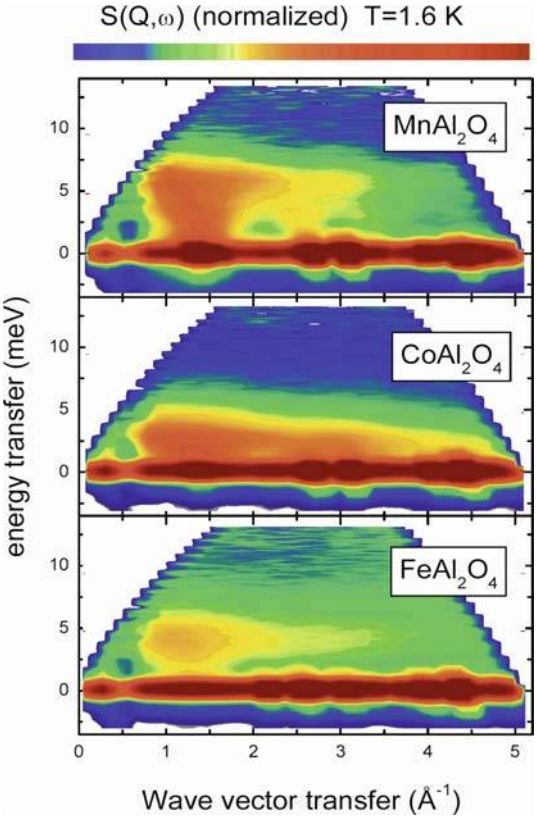

Figure 3 (online colour at: www.pss-a.com) Dynamic structure factor $S(Q, \omega)$ of MAl_2O_4 (M = Co, Fe, Mn) at $T = 1.6$ K. For details see text.

spite the absence of long-range magnetic order (middle frame of Fig. 3). Such behaviour corresponds to a cooperative paramagnet. For $FeAl_2O_4$, the opening of a spin gap is observed at low temperatures (lower frame of Fig. 3). These three A-site spinels are located at the border of the long-range magnetic order with distinct emergent behaviour [28].

3.3 Multiferroics The finding of the ferroelectricity and giant magnetocapacitance in magnetic perovskite rare-earth manganites [29–31] has revived the interest in this effect and stimulated the search for other materials with such prominent properties, termed multiferroics. Multiferroics exhibit the simultaneous occurrence of ferroelectricity and long-range magnetic order. Their investigation is a highly active topic in recent solid state research [32]. The mutual control of magnetic and ferroelectric polarization in multiferroic materials offers the possibility of realizing a new generation of magneto-electronic and magneto-optical devices. The giant magnetocapacitive coupling in perovskite manganites is suggested to arise from the correlation of the spin structure, lattice modulation and dielectric properties. It is well settled now that the polar order in these materials is associated with the formation of a complex magnetic structure involving a spiral magnetic state, driven by competing interactions and/or frustration, and some theoretical explanations of their multiferroicity along this line were recently proposed [33–35]. Multiferroic behaviour was recently found in other kinds of helimagnets, in which the magnetic propagation vector is perpendicular to the spin spiral plane. An electric polarization can be induced by an external magnetic field, as demonstrated in $ZnCr_2Se_4$ [36]. In contrast, colossal magnetocapacitive coupling is also found in the $CdCr_2S_4$ spinel, a compound with a simple ferromagnetic (FM) structure [12, 37]. The temperature dependence of the dielectric constant $\varepsilon'(T)$ in $CdCr_2S_4$ exhibits a steep rise below the Curie temperature T_C, driven by the onset of ferromagnetic order that indicates strong magnetoelectric coupling (Fig. 4). Close to the ferromagnetic ordering temperature at $T_C = 84.5$ K the magnetocapacitive coupling reaches colossal values of about 30 in a field of 100 kOe. On decreasing the temperature, the $\varepsilon'(T)$, shows a maximum followed by a decrease at lower temperatures reminiscent of ferroelectric behaviour. Its width and value of $\varepsilon \approx 100$ indicate a transition into a polar state of diffusive character. A finite ferroelectric polarization arises below T_C with a polarization cycle exhibiting a clear ferroelectric hysteresis. The relatively narrow hysteresis loop indicates a non-canonical ferroelectric behaviour. The character of the ferroelectric state is revealed from the temperature dependence of ε', which exhibits the characteristic behaviour of a relaxor ferroelectric, the typical strong dispersion effects being ascribed to the

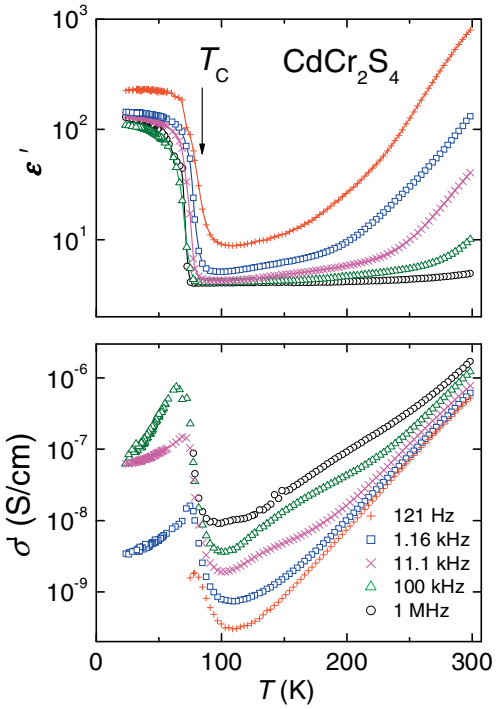

Figure 4 (online colour at: www.pss-a.com) Temperature dependences of the dielectric constant ε' and *ac* conductivity σ' at various frequencies for an electronically doped $CdCr_2S_4$ single crystal. The sample was prepared with bromine as transport agent instead of chlorine used in the original reports [12, 37].

freezing-in of ferroelectric clusters [38]. Most relaxor ferroelectrics known so far are perovskite-related materials where long-range polar order is suppressed by substitutional disorder. In contrast, the relaxor properties in $CdCr_2S_4$ appear in a compound without any structural disorder.

Even higher magnetocapacitive coupling was found in another compound, $HgCr_2S_4$, which manifests metamagnetic behaviour and complex spiral antiferromagnetic order below the Néel temperature $T_N = 22$ K [39], quite similar as in the multiferroic rare-earth manganites. The dielectric constant becomes strongly enhanced below 60 K, which is ascribed to polar dynamics governed by the onset of strong ferromagnetic correlations [13]. In addition, the observation of polarization hysteresis curves indicates the development of ferroelectric order below about 70 K. Investigations in external magnetic fields up to 50 kOe reveal the simultaneous occurrence of magnetocapacitance and magnetoresistance of colossal magnitudes in this material.

The appearance of the polar order is quite unexpected for spinel compounds with purely cubic lattice and indicates deviation from the cubic symmetry. Recent Raman experiments reported on the appearance of new modes, pointing to the local loss of inversion symmetry [40]. The nature of the polar moments is yet unclear. It is suggested to result from the off-center displacement of the Cr ions. At present, the origin of the colossal magnetocapacitive coupling and relaxor behaviour as well as the microscopic origin of the ferroelectric effect in the chromium chalcogenide spinels is far from being well understood, especially in $CdCr_2S_4$ where no spiral magnetic state is formed. The high sensitivity of the magnetocapacitive effect to details of sample stoichiometry and doping makes it difficult to uncover the dominant mechanism responsible for this effect. The results of Fig. 4 demonstrate that the effect is also present in samples prepared with Br as transport agent, which is less prone to enter the lattice than the chlorine used in the original reports [12, 37].

3.4 Spin-driven structural transformations In the $ZnCr_2S_4$ spinel with competing ferromagnetic and antiferromagnetic exchange interactions of almost equal strength, the magnetic susceptibility, specific heat, and thermal expansion reveal significant anomalies that accompany the two subsequent magnetic transitions to incommensurate spiral antiferromagnetic order at $T_{N1} = 15$ K and to commensurate collinear order at $T_{N2} = 8$ K [15]. Below T_{N1}, after a continuous drop, the susceptibility exhibits a sharp change of slope at around T_{N2}. In addition, a pronounced difference between the susceptibilities measured on cooling and heating was observed. Such irreversibility indicates a first-order transformation. Both magnetic anomalies are in good agreement with the early neutron-diffraction experiments [41, 42]. On approaching T_{N1}, the specific heat manifests a sharp lambda-like anomaly (Fig. 5a). On further decreasing temperature, a second maximum at T_{N2} becomes evident. It correlates with the respective anomaly observed in the susceptibility. At around T_{N2} a noticeable hysteresis in the specific heat is found by measurements on cooling and heating again pointing to a first- order transformation. We relate it to a structural transition which can be deduced from the thermal expansion data (Fig. 5b). The thermal expansion exhibits strong anomalies both at T_{N1} and T_{N2}. The application of a magnetic field has a strong effect on the specific heat C and the thermal expansion coefficient α shifting the maximum in C and α at T_{N1} to lower temperatures. At the same time, the peaks in C and α at T_{N2} become strongly suppressed above a critical field of 20 kOe and simultaneously exhibit shifts to lower temperatures.

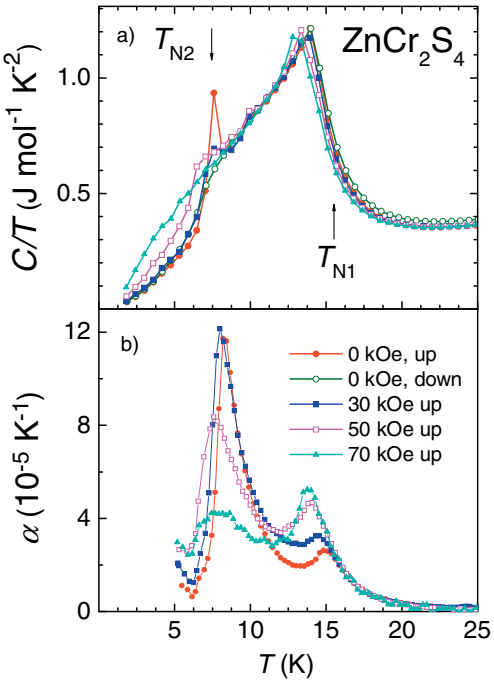

Figure 5 (online colour at: www.pss-a.com) (a) Heat capacity of $ZnCr_2S_4$, plotted as C/T vs. T at low temperatures measured on cooling (open circles) for zero field and warming (other symbols) for fields between 0 and 70 kOe. Magnetic transitions at T_{N1} and T_{N2} are indicated by arrows; (b) temperature dependences of the thermal expansion coefficient α at different external magnetic fields.

The IR reflectivity spectrum at room temperature (Fig. 6) reveals the four group-theoretically allowed IR-active phonon modes [43]. On decreasing temperature from 300 K down to 20 K, positive frequency shifts of the phonon eigenmodes were found which are attributed to purely anharmonic behaviour of a cubic spinel structure. Below the first magnetic transition into the helical structure at T_{N1} all main modes reveal an additional shift towards higher frequencies, as expected for AFM transitions. The shift is of the order of 1% for the high and of the order of 2% for the low-frequency modes. Below the magnetic transition temperatures all phonon modes show a clear splitting indicating a symmetry breaking. As one of the

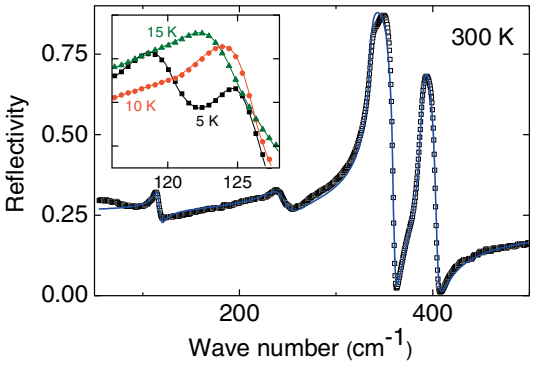

Figure 6 (online colour at: www.pss-a.com) Reflectivity spectrum for a $ZnCr_2S_4$ single crystal [15, 43]. The solid line is a fit with Lorentz oscillators. The inset shows an enlargement of the region of the lowest mode with the appearance of a new mode.

important results we note that the phonon splitting at T_{N2} is suppressed in high magnetic fields. Together with the similar field behaviour of the anomalies in the specific heat and in the thermal expansion this evidences a spin-driven origin of the structural transformation at T_{N1} and T_{N2}.

The splitting of the IR-active modes in $ZnCr_2S_4$ at the two magnetic phase transitions supports the interpretation of this effect as due to competing ferromagnetic and antiferromagnetic exchange interactions. The high-frequency phonon modes involve vibrations mostly of Cr–S units. The FM 90° Cr–S–Cr exchange governs the order of FM (001) planes. This exchange interaction is responsible for the splitting of the high-frequency modes. However, $ZnCr_2S_4$ is also equally dominated by the AFM exchange which establishes the complex commensurate collinear spin order. These AFM interactions comprise mainly Zn–S bonds which on the other side are involved in the eigenfrequencies of the low-lying phonon modes. Consequently, at T_{N2} these modes are expected to split as experimentally observed.

The comparable splitting of both high- and low-frequency modes provides evidence that FM and AFM exchange interactions are of equal strength. The ground state energies of the two spin configurations are similar and the transition into the low-temperature phase is generated by these competing interactions. Thus, the experiments suggest that the low-temperature symmetry breaking in the $ZnCr_2S_4$ spinel mainly results from a strong spin-phonon coupling [43]. Recent high-resolution synchrotron powder diffraction of $ZnCr_2S_4$ revealed two consequent structural transformations from a cubic to a tetragonally distorted intermediate phase below T_{N1} and a further transition to a low-temperature orthorhombic phase below T_{N2} [44] in agreement with these expectations.

In the $ZnCr_2Se_4$ spinel which is dominated by strong ferromagnetic exchange ($\Theta_{CW} = 100$ K) but orders antiferromagnetically at $T_N = 21$ K, the specific heat and thermal expansion exhibit sharp first-order anomalies at the antiferromagnetic transition (Fig. 7) [14]. The transition temperature as well as the anomalies in the specific heat

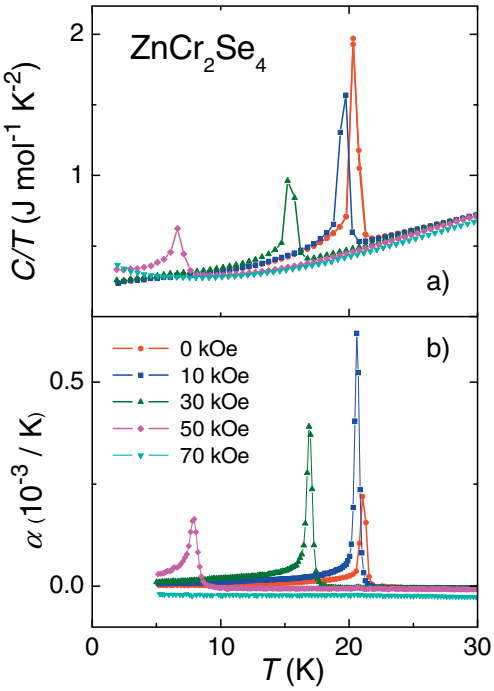

Figure 7 (online colour at: www.pss-a.com) (a) Temperature dependence of the heat capacity of a $ZnCr_2Se_4$ single crystal plotted as C/T vs. T; (b) temperature dependence of the thermal expansion coefficient α at various magnetic fields between 0 kOe and 70 kOe applied along the ⟨001⟩ axis.

and thermal expansion are shifted to lower temperatures by external magnetic field and, finally, antiferromagnetic order becomes suppressed by a field of 65 kOe.

The relative length change of the samples $\Delta L/L(T)$ is unusually large and exhibits negative thermal expansion below 75 K down to T_N indicating strong frustration of the lattice (Fig. 8a). The magnetostriction $\Delta L/L(H)$ reveals large values comparable to giant magnetostrictive materials (Fig. 8b).

The obtained data reveal a strong spin–lattice coupling and evidence a spin-driven origin of the structural transformation from the high-temperature cubic phase to a lower symmetry below the magnetic transition at T_N. The dominant magnetic coupling mechanism in $ZnCr_2Se_4$ is superexchange, which includes FM Cr–Se–Cr and AFM Cr–Se–Zn–Se–Cr or Cr–Se–Se–Cr exchange interactions. These competing interactions establish a complex spin configuration. The FM 90° Cr–Se–Cr exchange governs the ferromagnetic order in the (001) planes. The AFM exchange is probably responsible for the spin arrangement between the adjacent (001) planes. An external magnetic field changes the balance between FM and AFM interactions enhancing the ferromagnetic correlations and reduces the angle between the spins in the adjacent FM planes. In agreement with the observation of the concomitant reduction of the anomalies of specific heat and thermal expansion by a magnetic field, this corroborates the interpretation of the low-temperature structural symmetry breaking

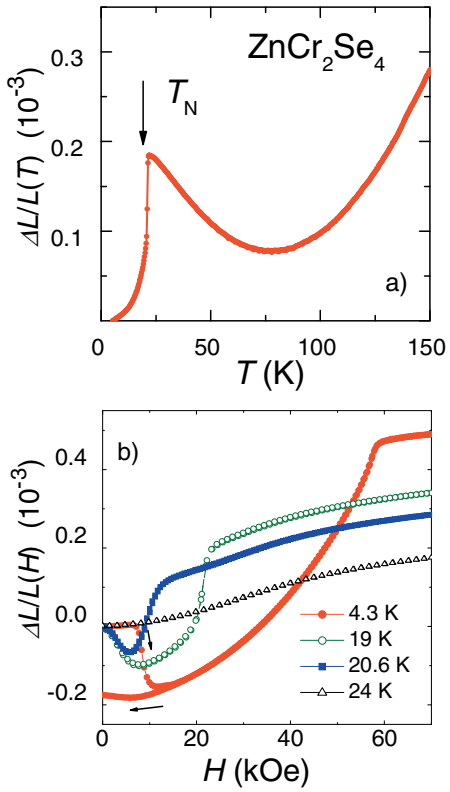

Figure 8 (online colour at: www.pss-a.com) (a) Temperature dependence of the thermal expansion $\Delta L/L(T)$ for a $ZnCr_2Se_4$ single crystal at different external magnetic fields; (b) Longitudinal magnetostriction $\Delta L/L(H)$ at different temperatures below and above T_N.

in $ZnCr_2Se_4$ as due to bond frustration caused by competing exchange. This results in an extremely large influence of the magnetic field on the structural transition. The negative thermal expansion indicates strong frustration of the highly symmetric lattice in the paramagnetic regime. This frustrated lattice is highly receptive to weak perturbations which are primarily induced by magnetic order at T_N. The coupling between magnetism and lattice may be realized via an exchange-striction mechanism similar to a spin-Peierls transition.

In the absence of magnetic field the IR-optical investigations of $ZnCr_2Se_4$ found an increase of the phonon eigenfrequencies with decreasing temperature as usually observed in anharmonic crystals [16]. However, all modes reveal significant deviations from the purely anharmonic behaviour for $T < 100$ K. The deviations are positive for mode 1, but negative for modes 2 and 4. The anomalous temperature dependence evolves below 100 K, at a temperature scale corresponding to the Curie–Weiss temperature $\Theta_{CW} = 100$ K, and becomes strongly enhanced just below T_N. In addition, the lowest mode 1 manifests a clear splitting below the antiferromagnetic phase transition at $T_N = 21$ K.

The reflectivity data taken at 5 K in an external magnetic field of 70 kOe revealed only minor changes for the high-frequency modes 3 and 4, while significant shifts are obtained for the phonon modes 1 and 2. The most important observation is the complete suppression of the splitting of mode 1 by magnetic field, underlining the spin-driven origin of the structural transformation.

4 Conclusion Recent experimental studies of magnetic semiconductor spinels demonstrate important achievements in physics and technology. Our detailed magnetic, thermal, dielectric, and IR spectroscopy investigations of ternary magnetic oxide and chalcogenide spinels AB_2X_4 (A = Fe, Mn, Co, Cd, Zn, Hg; B = Cr, Co, Sc, Al; X = O, S, Se) revealed highly correlated spin, charge, orbital, and lattice degrees of freedom in these compounds.

The obtained results evidence the novel ground states, like spin liquid, spin–orbital liquid and orbital glass originating from strong spin and orbital frustration. Several colossal response functions driven by the onset of the magnetic order, e.g., colossal magnetoresistance, colossal magnetocapacitive coupling and colossal magnetostriction were revealed. Intricate phenomena, like negative thermal expansion and splitting of the phonon modes associated with the spin-driven Jahn–Teller structural transformations are found. The obtained results prove that the low-temperature symmetry breaking in the investigated chalcogenide spinels despite negligible spin–orbit coupling stems from strong spin-phonon coupling. Bond frustration caused by competing ferromagnetic and antiferromagnetic exchange interactions is believed to generate this remarkable behaviour.

Acknowledgements This work has been supported by the Deutsche Forschungsgemeinschaft (DFG) via the collaborative research center SFB 484 (Augsburg). The support via Grant 08.820.05.038RF within the collaborative agreement of the Academy of Science of Moldova and Russian Science Support Foundation is also acknowledged.

References

[1] S. Kondo, D. C. Johnston, C. A. Swenson, F. Borsa, A. V. Mahajan, L. L. Miller, T. Gu, A. I. Goldman, M. B. Maple, D. A. Gajewski, E. J. Freeman, N. R. Dilley, R. P. Dickey, J. Merrin, K. Kojima, G. M. Luke, Y. J. Uemura, O. Chmaissem, and J. D. Jorgensen, Phys. Rev. Lett. **78**, 3729 (1997).

[2] A. Krimmel, A. Loidl, M. Klemm, S. Horn, and H. Schober, Phys. Rev. Lett. **82**, 2919 (1999).

[3] A. P. Ramirez, R. J. Cava, and J. Krajewski, Nature (London) **386**, 156 (1997).

[4] V. Fritsch, J. Deisenhofer, R. Fichtl, J. Hemberger, H.-A. Krug von Nidda, M. Mücksch, M. Nicklas, D. Samusi, J. D. Thompson, R. Tidecks, V. Tsurkan, and A. Loidl, Phys. Rev. B **67**, 144419 (2003).

[5] S.-H. Lee, C. Broholm, W. Ratcliff II, G. Gasparovic, Q. Huang, T. H. Kim, and S.-W. Cheong, Nature (London) **418**, 856 (2002).

[6] P. G. Radaelli, Y. Horibe, M. J. Gutmann, H. Ishibashi, C. H. Chen, R. M. Ibberson, Y. Koyama, Y. S. Hor,

V. Kiryukhin, and S.-W. Cheong, Nature (London) **416**, 155 (2002).
[7] M. Schmidt, W. Ratcliff II, P. G. Radaelli, K. Refson, N. M. Harrison, and S.-W. Cheong, Phys. Rev. Lett. **92**, 056402 (2004).
[8] K. Ohgushi, T. Ogasawara, Y. Okimoto, S. Miyasaka, and Y. Tokura, Phys. Rev. B **72**, 155114 (2005).
[9] R. Fichtl, V. Tsurkan, P. Lunkenheimer, J. Hemberger, V. Fritsch, H.-A. Krug von Nidda, E.-W. Scheidt, and A. Loidl, Phys. Rev. Lett. **94**, 027601 (2005).
[10] V. Tsurkan, V. Fritsch, J. Hemberger, H.-A. Krug von Nidda, D. Samusi, S. Körner, E.-W. Scheidt, S. Horn, R. Tidecks, and A. Loidl, J. Phys. Chem. Solids **66**, 2036 (2005).
[11] V. Fritsch, J. Hemberger, N. Büttgen, E.-W. Scheidt, H.-A. Krug von Nidda, A. Loidl, and V. Tsurkan, Phys. Rev. Lett. **92**, 116401 (2004).
[12] J. Hemberger, P. Lunkenheimer, R. Fichtl, H.-A. Krug von Nidda, V. Tsurkan, and A. Loidl, Nature (London) **434**, 364 (2005).
[13] S. Weber, P. Lunkenheimer, R. Fichtl, J. Hemberger, V. Tsurkan, and A. Loidl, Phys. Rev. Lett. **96**, 157202 (2006).
[14] J. Hemberger, H.-A. Krug von Nidda, V. Tsurkan, and A. Loidl, Phys. Rev. Lett. **98**, 147203 (2007).
[15] J. Hemberger, T. Rudolf, H.-A. Krug von Nidda, F. Mayr, A. Pimenov, V. Tsurkan, and A. Loidl, Phys. Rev. Lett. **97**, 087204 (2006).
[16] T. Rudolf, C. Kant, F. Mayr, J. Hemberger, V. Tsurkan, and A. Loidl, Phys. Rev. B **75**, 052410 (2007).
[17] S.-H. Lee, C. Broholm, T. H. Kim, W. Ratcliff II, and S.-W. Cheong, Phys. Rev. Lett. **84**, 3718 (2000).
[18] O. Tchernyshyov, R. Moessner, and S. L. Sondhi, Phys. Rev. Lett. **88**, 067203 (2002).
[19] O. Tchernyshyov, R. Moessner, and S. L. Sondhi, Phys. Rev. B **66**, 064403 (2002).
[20] P. W. Anderson, Phys. Rev. **102**, 1008 (1956).
[21] N. Tristan, J. Hemberger, A. Krimmel, H.-A. Krug von Nidda, V. Tsurkan, and A. Loidl, Phys. Rev. B **72**, 174404 (2005).
[22] D. Bergman, J. Alicea, E. Gull, S. Trebst, and L. Balents, Nature Physics **3**, 487 (2007).
[23] V. Zestrea, V. Y. Kodash, V. Felea, P. Petrenco, D. V. Quach, J. R. Groza, and V. Tsurkan, J. Mater. Sci. **43**, 660 (2008).
[24] N. Tristan, V. Zestrea, G. Behr, R. Klingeler, B. Büchner, H.-A. Krug von Nidda, A. Loidl, and V. Tsurkan, Phys. Rev. B **77**, 094412 (2008).
[25] A. Krimmel, M. Mücksch, V. Tsurkan, M. M. Koza, H. Mutka, and A. Loidl, Phys. Rev. Lett. **94**, 237402 (2005).
[26] A. Krimmel, M. Mücksch, V. Tsurkan, M. M. Koza, H. Mutka, C. Ritter, D. V. Sheptyakov, S. Horn, and A. Loidl, Phys. Rev. B **73**, 014413 (2006).
[27] A. Krimmel, V. Tsurkan, D. Sheptyakov, and A. Loidl, Physica B **378–380**, 583 (2006).
[28] A. Krimmel, H. Mutka, M. M. Koza, V. Tsurkan, and A. Loidl, in press (2008).
[29] T. Kimura, T. Goto, H. Shintani, K. Ishizaka, T. Arima, and Y. Tokura, Nature (London) **426**, 55 (2003).
[30] T. Goto, T. Kimura, G. Lawes, A. P. Ramirez, and Y. Tokura, Phys. Rev. Lett. **92**, 257201 (2004).
[31] N. Hur, S. Park, P. A. Sharma, S. Guha, and S.-W. Cheong, Phys. Rev. Lett. **93**, 107207 (2004).
[32] N. A. Spaldin and M. Fiebig, Science **391**, 5733 (2005).
[33] H. Katsura, N. Nagaosa, and A. V. Balatsky, Phys. Rev. Lett. **95**, 057205 (2005).
[34] I. A. Sergienko and E. Dagotto, Phys. Rev. B **73**, 094434 (2006).
[35] M. Mostovoy, Phys. Rev. Lett. **96**, 067601 (2006).
[36] H. Murakawa, Y. Onose, K. Ohgushi, S. Ishiwata, and Y. Tokura, J. Phys. Soc. Jpn. **77**, 043709 (2008).
[37] P. Lunkenheimer, R. Fichtl, J. Hemberger, V. Tsurkan, and A. Loidl, Phys. Rev. B **72**, 060103(R) (2005).
[38] J. Hemberger, P. Lunkenheimer, R. Fichtl, S. Weber, V. Tsurkan, and A. Loidl, Phase Transit. **79**, 1065 (2006).
[39] V. Tsurkan, J. Hemberger, A. Krimmel, H.-A. Krug von Nidda, P. Lunkenheimer, S. Weber, V. Zestrea, and A. Loidl, Phys. Rev. B **73**, 224442 (2006).
[40] V. Gnezdilov, P. Lemmens, Yu. G. Pashkevich, P. Scheib, Ch. Payen, K. Y. Choi, J. Hemberger, A. Loidl, and V. Tsurkan, arXiv: cond-mat 0702362 (2007).
[41] M. Hamedoun, A. Wierdenmann, J. L. Dormann, M. Nogues, and J. Rossat-Mignod, J. Phys. C **19**, 1783 (1986).
[42] M. Hamedoun, A. Wierdenmann, J. L. Dormann, M. Nogues, and J. Rossat-Mignod, J. Phys. C **19**, 1801 (1986).
[43] T. Rudolf, C. Kant, F. Mayr, J. Hemberger, V. Tsurkan, and A. Loidl, New J. Phys. **9**, 76 (2007).
[44] F. Yokaichiya, A. Krimmel, V. Tsurkan, I. Margiolaki, P. Thompson, H. N. Bordallo, A. Buchsteiner, N. Stüßer, D. N. Argyriou, and A. Loidl, in press (2008).